SCIENCE CHINA
Physics, Mechanics & Astronomy

• Invited Review •

March 2017 Vol. 60 No. 3: 034201
doi: 10.1007/s11433-016-0447-6

Two-photon reduction: a cost-effective method for fabrication of functional metallic nanostructures

Sahar Tabrizi, YaoYu Cao, Han Lin, and BaoHua Jia*

Centre for Micro-Photonics, Faculty of Science, Engineering and Technology, Swinburne University of Technology, Hawthorn, Victoria 3122, Australia

Received November 9, 2016; accepted January 3, 2017; published online January 13, 2017

Metallic nanostructures have underpinned plasmonic-based advanced photonic devices in a broad range of research fields over the last decade including physics, engineering, material science and bioscience. The key to realizing functional plasmonic resonances that can manipulate light at the optical frequencies relies on the creation of conductive metallic structures at the nanoscale with low structural defects. Currently, most plasmonic nanostructures are fabricated either by electron beam lithography (EBL) or by focused ion beam (FIB) milling, which are expensive, complicated and time-consuming. In comparison, the direct laser writing (DLW) technique has demonstrated its high spatial resolution and cost-effectiveness in three-dimensional fabrication of micro/nanostructures. Furthermore, the recent breakthroughs in superresolution nanofabrication and parallel writing have significantly advanced the fabrication resolution and throughput of the DLW method and made it one of the promising future nanofabrication technologies with low-cost and scalability. In this review, we provide a comprehensive summary of the state-of-the-art DLW fabrication technology for nanometer scale metallic structures. The fabrication mechanisms, different material choices, fabrication capability, including resolution, conductivity and structure surface smoothness, as well as the characterization methods and achievable devices for different applications are presented. In particular, the development trends of the field and the perspectives for future opportunities and challenges are provided at the end of the review. It has been demonstrated that the quality of the metallic structures fabricated using the DLW method is excellent compared with other methods providing a new and enabling platform for functional nanophotonic device fabrication.

two photon photoreduction, metallic nanostructures, nanofabrication, plasmonics

PACS number(s): 42.25.Bs, 42.25.Ja, 42.65.Re

Citation: S. Tabrizi, Y. Y. Cao, H. Lin, and B. H. Jia, Two-photon reduction: a cost-effective method for fabrication of functional metallic nanostructures, Sci. China-Phys. Mech. Astron. **60**, 034201 (2017), doi: 10.1007/s11433-016-0447-6

1 Introduction

Metallic micro/nanostructures have free electrons flowing on the surface that create surface plasmon polaritons (SPP) through which electromagnetic (EM) field can be controlled and localized in a nano-scale. This property makes metallic nanostructures competent candidates for broad research fields such as metallic photonics crystals, metamaterials, plasmonic structures, microfluidic chips and also surface-enhanced Raman scattering (SERS) because metallic nanostructures are capable of controlling the optical energy in a sub-wavelength region [1-9].

To achieve functionalities for different applications, metallic micro/nanostructures need to meet several key requirements. Firstly, micro/nanostructures need to possess a high

*Corresponding author (email: bjia@swin.edu.au)

conductivity since high free electron mobility could increase surface plasmons formation; Secondly, the structures are required to be in the sub-wavelength range, since the working wavelengths of the devices are proportional to the structure feature size. For instance, to achieve plasmonic devices in the optical regime, structure feature down to a few hundreds of nanometre are required. Finally, to realize the maximum spatial confinement, three dimensional (3D) micro/nanostructures are required. However, simultaneously satisfying these conditions, which means fabrication of 3D highly conductive metallic micro/nanostructures with a small-feature-size down to the nanometer scale, is challenging. But it holds the key for diverse applications in electronics and nanophotonics [10,11].

Advances in fabrication accuracy and resolution require improvement in fabrication methods. Great progress in decreasing the metallic feature size to nano-scale has been achieved via nanofabrication techniques such as excimer laser lithography, nanoimprinting lithography, focused ion beam (FIB) milling, electron beam lithography (EBL) and plasmonic lithography [12-19]. However, these nanofabrication processes involve multiple steps including patterning of photoresist, metal deposition and removal of the photoresist, which are not only complex and time-consuming, but also somehow degrade the quality of the fabricated structures. More importantly, it becomes extremely challenging for the fabrication of 3D metallic structures using these methods because neither the method is capable of 3D direct fabrication. On the other hand, using alignment in 3D is far more too complicated.

Recently, direct laser writing (DLW) has achieved enormous successes due to its capability of one-step fabrication of arbitrary 3D micro/nanostructures with high throughput and high resolution in a broad range of materials, including dielectrics and metals [5,20-27]. Applying an ultrafast laser in DLW method, we are able to focus the ultrafast laser beam tightly into a tiny spot, in which the chemical reactions of materials are controlled via the multiphoton absorption process that enables the fabrication of micro/nanostructures with complex geometries [25-33]. Due to the 3D confinement of the nonlinear multiphoton absorption only in the focal region and the material threshold response, high spatial resolution surpassing the diffraction limit can be achieved [34]. In addition, the detrimental thermal effect that degrades the spatial resolution can be minimized by controlling the pulse width and the repetition rate of the ultrafast laser [35].

To realize functional metallic micro/nanostructures different DLW approaches have been demonstrated, such as the coating method, the inversion method [36] and the photoreduction method [36-40]. Both the coating and inversion methods depend on a multistep procedure and start with the DLW of polymer templates followed by either a solution based metal layer coating process [37,41] or a chemical vapor deposition or electrochemical deposition inversion process. Eventually, the polymer templates are removed by the etching technique, as shown in Figure 1(b) [36].

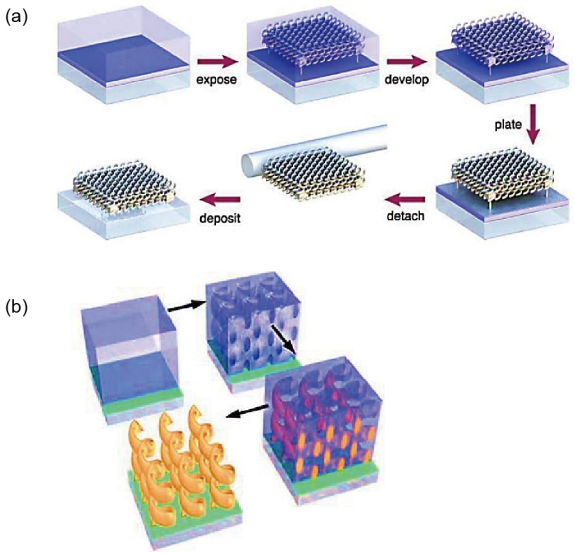

Figure 1 (Color online) (a) Fabrication scheme of the templating coating method. A glass cover slip serves as the substrate on which a double layer of negative-tone photoresist is deposited via spincoating. The thinner bottom layer is pre-crosslinked by UV flood exposure and serves as an adhesion layer. The top layer is exposed via 3D direct laser writing. Post-baking and developing converts the latent image formed during the exposure into a free-standing photoresist template of a 3D bichiral crystal resting on four small posts, one at each corner. All surfaces of this template as well as the adhesion layer are coated with a conformal silver film via electroless plating. To facilitate transmission spectroscopy, the bichiral crystal is detached from the silvered substrate with a thin glass capillary and deposited on a clean glass cover slip [8]. (b) Fabrication scheme of inversion method. A positive-tone photoresist (blue) is spun onto a glass substrate covered with a 25-nm thin film of conductive indium-tin oxide (ITO) shown in green. After 3D DLW and development, an array of air helices in a block of polymer results. After plating with gold in an electrolyte, the polymer is removed by plasma etching, leading to a square array of freestanding 3D gold helices [36].

With these methods, even the polymer templates have adequate quality, it remains challenging to achieve a uniform coating or complete infiltration due to the complicated 3D micro/nanoenvironment of the fabricated structures. Furthermore, such coatings and inversions do not normally maintain the exact geometry of the original templates due to the harsh procedures involved, which tends to attack the templates. Compared to the two-step templating methods, the single-step photoreduction method can directly fabricate 3D metallic micro/nanostructures from solution with a great simplicity using the multiphoton reduction mechanism [23-32]. However, due to the structure formation mechanism, which is based on the nucleation of small nanoparticles (NPs), the current challenges in this method lie in the realization of high-resolution metallic structures with small surface roughness and high electrical conductivity towards functional plasmonic nanostructures with resonances in the optical regime.

Recently, highly sensitive two-photon reduction (2PR) technique [41-46] has been developed to fabricate conductive

3D micro/nanostructures in one step with high flexibility and efficiency. It has been demonstrated that the quality of the metallic structures fabricated using the 2PR method is excellent compared with other methods [47] providing a new and enabling platform for functional nanophotonic device fabrication. In this manuscript, we provide a comprehensive review of the development of the 2PR method for the fabrication of metallic structures. We introduce the 2PR method as a cost-effective nanofabrication approach for realizing functional metallic micro/nanostructures in the optical regime in sect. 2. We discuss the material properties and the fabrication threshold in sect. 3. The fabrication parameters and characterization regarding conductivity and smoothness of the fabricated structures are presented in sect. 4. The potential and relevant applications, remaining challenges and future prospects of the 2PR method are given in sect. 5.

2 Two-photon photoreduction process

2PR process is realized when two photons are absorbed, simultaneously—weather being identical or different in frequencies—to excite a molecule to a higher energy level as it is shown in Figure 2. The amount of energy for both photons should be equal to the energy difference between two energy states of the molecule. Two-photon absorption is known as a third order nonlinear procedure depends on the square of the light intensity [48], which is much weaker than the linear absorption that happens at low light intensity. So, through the multiphoton photoreduction process, a metal ion absorbs two or more photons simultaneously to be reduced into metal NPs.

According to the literature, the basic mechanism for photoreduction of metal ions is the absorption of two photons by the metal ions either through the molecules of a dye material

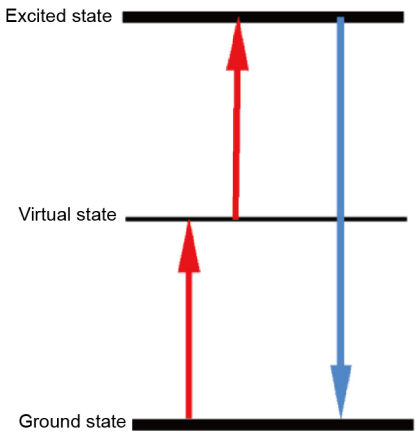

Figure 2 (Color online) Schematic of energy states of two-photon excitation process [49].

such as 2-hydroxy-4'-(2-hydroxyethoxy)-2-methylpropiophenone (HHMP) [47], which will act as a photosensitizer in the process or directly from a laser beam [39]. In the case of using dye material in the 2PR solution, transferring of an electron from the excited dye to the metal ion leads to the form-ation of a metal atom, which can either (a) react with other metal atoms to nucleate, or (b) add onto an existing particle, or (c) undergo a charge combination [47,50].

Thus the formation and growth of metal particles are limited by the competition between the rate of growth or nucleation and charge recombination, as well as local depletion of metal ions. Since the growth rate is generally much greater than the nucleation rate and it depends on the number of nucleation centres, it is reasonable to state that the introduction of NPs seeds into the composite could significantly enhance the formation efficiency of a continuous metal phase. The photoreduction of the metal nanostructures can be divided into three stages: nucleation, growth, and aggregation of metal NPs to form micro/nanostructures.

The single-photon absorption rate is measured using the Beer's law [51] as shown in eq. (1). For 2PR process this law is still valid but it needs to be modified to eq. (2). The light intensity is a function of the path length (x), the concentration c and the initial light intensity (I_0). α and β are the absorption coefficients of one and 2PR processes, consequently [52].

$$I(x) = I_0 \mathrm{e}^{-\alpha c x}, \tag{1}$$

$$I(x) = \frac{I_0}{1+\beta c x I_0}. \tag{2}$$

To excite the two-photon absorption (TPA) in the TPR process, tightly focused ultrafast laser pulses have to be employed. Ultrafast laser has the ability to transfer a massive amount of photon energy (with a peak power on the order of ~10^{14} W/cm^2) in a small fraction of the time [53]. In other words, the photon energy could be deposited in the lattice much faster while the material is exposed to the femtosecond pulses compared to the energy transformation with electrons through phonon emission. This is especially beneficial in TPR in which thermal diffusion effect can impose a negative impact on the fabrication resolution [31,34,54,55].

A typical setup for the 2PR fabrication of metallic structures is shown in Figure 3(a). Femtosecond laser pulses first pass a neutral density (ND) filter, where the beam intensity could be properly adjusted. A beam expansion system allows the uniform illumination over the back aperture of a high numerical aperture (NA) objective lens. The laser beam could be tightly focused into the photoreduction solution in a nanometric volume on the order of $\lambda^3/4$ (λ is the wavelength of the incident light) by the high NA objective lens as shown Figure 3(b). The beam is focused into a sample to initiate the photoreduction. The sample, the photoreduction solution, is often sandwiched between two coverslips as sho-

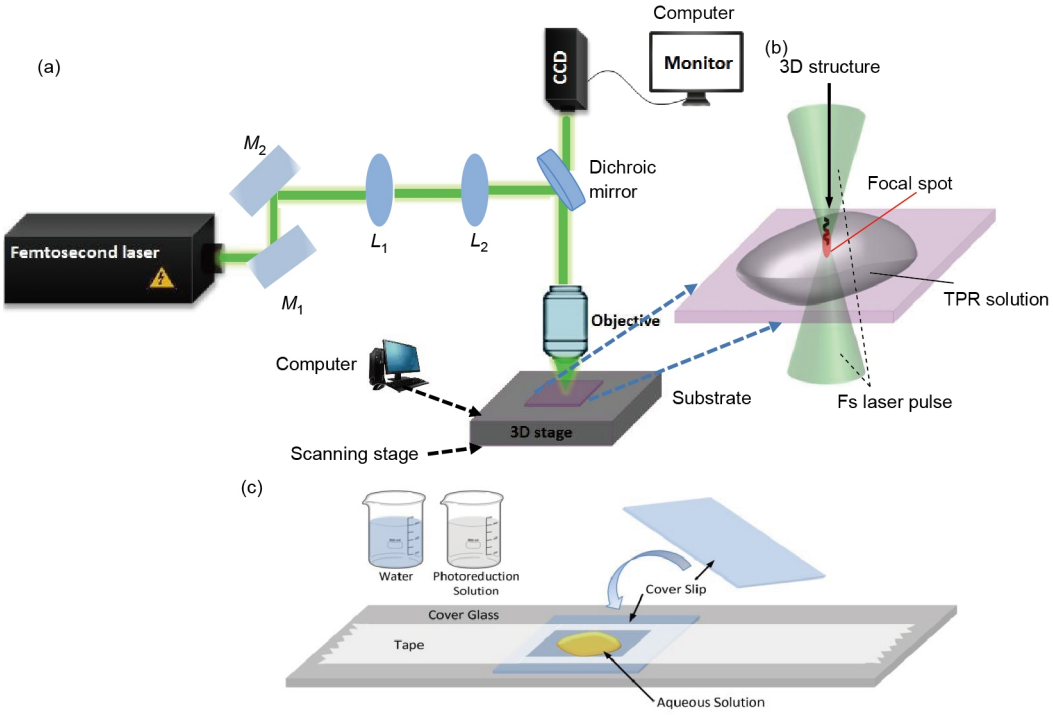

Figure 3 (Color online) (a) Schematic apparatus of laser 2PR system used in our experiment, M: mirror; L: lense. (b) Detailed configuration of the sample for the bottom-up fabrication of 3D structures. (c) Schematic of material preparation for photoreduction fabrication.

wn in Figure 3(c), which are separated with a sticky tape with a thickness in ~ 100-200 mm range. A 3D piezoelectric scanning stage, which supports the sample, provides the 3D precise movement on the subnanometer scale [2,29,30,39,56]. The motion of the scanning stage is pre-programmed and controlled by a computer to form desired 3D micro/nanostructures. The fabrication process is monitored in a real time by a charge-coupled device (CCD). The requirements for photoreduction materials are discussed in sect. 3. After the fabrication, the sample is developed through a simple post-processing procedure to achieve the stand-alone metallic micro/nanostructures.

There are two types of photoreduction processes, one is the photosensitized method developed by means of dye molecules in 2PR solution and the other is the non-photosensitized process. In the former route, the TPR process starts from the absorption of two photons simultaneously by the molecules of the photosensitisers, which can initiate the reduction of the metal ions into metal NPs as shown in Figure 4(a). Then electrons transfer from the lowest unoccupied molecule orbital level of the excited photosensitizer to the metal ions and create silver atoms. The generated metal atoms could either link with other metal atoms and nucleate or undergo charge recombination. As the growth rate of metal NPs is much faster than that of nucleation, metal poly-crystal grows continuously inside the laser spot through three main sequential reactions by tunning the focal spot in the material [50]. Figure 4(b) shows a schematic of the typical reduction process of metal ions. The presence of photosensitizer in the photoreduction solution enhances the electron transferring process to the metal ions leading to an increase in the formation of metal atoms.

Consequently, nucleation process speeds up due to the improved interaction between metal atoms [57]. This is a photochemical synthesis process through which the structures can be fabricated in different environments like the surfactant micelles in aqueous solution. During the creation of NPs, they could act as a stabilizing polymer to control the size and shape of the NPs [39,58]. The main benefits of this technique are the high spatial resolution, fast process, efficient formation of NPs and also the ability to control the incident light wavelength since it depends on the sensitizer rather than the metal source [12,58].

In the latter case, the nucleation process initiates with the absorption of photons by metal ions. Then silver nuclei grow up to create silver NPs and ultimately, aggregation of NPs with different non-uniform shapes and sizes form the final pattern [39]. Hence, the TPR mechanism could be defined in three different steps: first, the creation of seeds due to the reduction of silver ions in a laser focal spot; second, the growth of silver seeds to NPs and last, the aggregation of NPs, which form the silver pattern eventually as shown in Figure 4(b).

This process contains fundamental route of chemical reactions, which allows the laser light to interact directly with atoms or molecules. Through changing the material or tunning the conditions of the incident light, it is possible to make different modifications inside the material. In particular, due to the threshold behavior of the 2PR process, resolution bey-

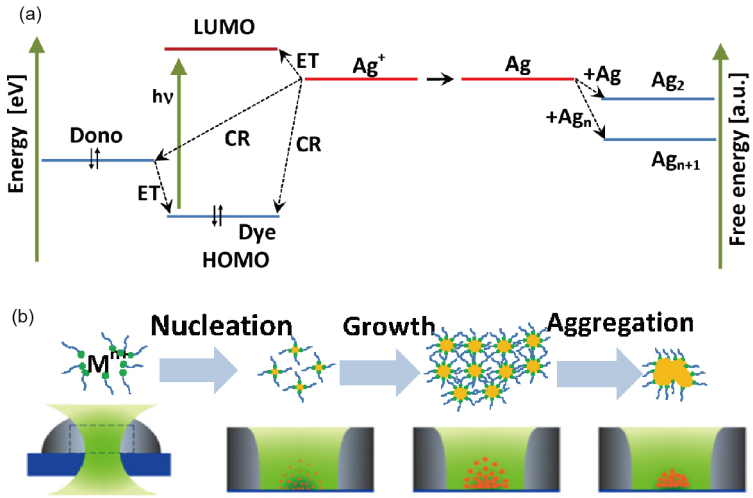

Figure 4 (Color online) (a) The basic scheme of photoinduced transfer from the dye molecules to metal ions for the reduction of metal ions. Symbols denote Ag^+, silver ion; Ag, silver atom; ET, the electron transfer; CR, charge recombination; HOMO, the highest occupied molecular orbital; LUMO, the lowest unoccupied molecular orbital. (b) Schematic of photoreduction process of metal ions and forming a metallic pattern in three steps; first, nucleation; second growing; final step, aggregation [39].

ond the diffraction limit can be realized by controlling the laser pulse energy and the number of applied pulses. Therefore, to achieve the best fabrication outcomes, the laser parameters, including the wavelength, pulse width, repetition rate, power level and scanning speed need to be optimized.

As shown in Table 1, most of the TPR experiments employed near infrared (NIR) femtosecond laser pulses readily from a Ti:Sapphire laser. However, it has been found that the laser illumination wavelength has a profound impact on the fabrication resolutions in two ways.

First of all, the Abbe's diffraction limit [59] is proportional to the illumination wavelength, the shorter the wavelength, the higher the achievable resolution given the two-photon absorption condition is still satisfied. Due to this reason, some groups introduced optical parametric oscillator (OPO) to convert the NIR femtosecond pulses to the visible ones, which has improved the fabrication resolution significantly [27,54,60-63]. Secondly, tuning the wavelength of the femtosecond laser can increase the photosensitivity of the photoreduction solution therefore significantly reducing the required threshold power leading to a much smaller fabricated feature size. It has been demonstrated by tuning the laser wavelength from 800 to 580 nm, the weight of the reduced silver dot fabricated with the laser energy in the threshold region increased faster with increasing the laser energy, which suggested that the shorter wavelength rendered a higher photosensitivity [12]. As a result, the fabricated feature size of the silver dot decreased from 220 to 130 nm. Through combining with the threshold fabrication mechanism and a highly photosensitive photoreduction medium the fabrication of the silver dot as small as 22 nm, which is equivalent to $\lambda/26$, far beyond the diffraction limit, has been achieved [12,34]. This result is by far the highest resolution achieved for silver dot fabrication. For line fabrication, the minimum line width of 120 nm was reported by Ishikawa [50], as summarized in Table 1.

At a given laser wavelength, the laser power and scanning speed are normally used to control the fabrication conditions and provide the essential energy to achieve different sized fabrication results. At an energy level higher than the threshold, the fabrication feature size normally has a monotonic dependence on the laser power or scanning speed when one of the parameters is fixed. The feature size increases with elevated power and reduced speed and reaches saturation at a certain level. According to the results presented by Maruo et al. [38] in 2008, the linewidth can be controlled precisely from 0.2 to 1.7 μm when the power is changed from 1 to 5 mW, as shown in Figure 5. On the other hand, increasing the scanning speed from 1 to ~100 μm/s at a constant fabrication power of 4 mW, resulting in the reduction in the linewidth from 1.2 to 0.3 μm. In this experiment, a Ti: sapphire laser of 752 nm wavelength with a pulse width of 200 fs and a repetition rate of 76 MHz was used. The objective had a NA of 1.25. Depending on the repetition rate of the fabrication laser, too high scanning speed can lead to discontinued lines due to the long time interval between two consecutive pulses. Therefore, to ensure high quality and comparatively fast fabrication, the scanning speed is normally maintained at a medium level while varying the laser power to adjust the fabrication feature size.

Laser pulse width and repetition rate are the two parameters that affect the thermal effect in the DLW fabrication and have been less discussed in 2PR. The laser pulse width can impact the fabrication feature size in two ways. On one hand, decreasing the pulse width increases the peak intensity at a constant power. Therefore, the photon density in the focal region

Table 1 Classification of past studies

Year/Group /Journal	Materials	Structure	Functionality	Resolution	Subject	Beam specification	Resistivity
2006/Castellana/Anal. Chem. [109]	Ag nanoparticle film/inside PDMS/TiO2	lines	lab on chip (LoC)/biosensors, screening assays	~10 μm	NP films inside sealed microfluidic channels	11 mW/cm^2 near 365 nm (UV)	NA
2006/Tanaka /Appl. Phys. Lett. [40]	silver-gold	line-ring-3D gate	arbitrary 3D structures	Line Au=700 nm vortex=1.02 μm	precise control of the laser power/laser power and linewidth is not linear	800 nm, 80 fs, 80 MHz, NA=1.42	5.3×10^{-8} Ω m
2006/Ishikawa/Appl. Phys. Lett. [70]	silver	line-3D cup	arbitrary 3D structures	400 nm	using two-photon sensitive dye to improve the reduction properties (electrical properties)	800 nm, 80 fs, 82 MHz, NA=1.42	NA
2007/Maruo/Opt.Express [110]	Polymer film containing Ag ions (3.8wt% & 3.8wt%)	line/pyramidal	Gratings, plasmonic devices/MEMS	*h*: 3 μm linewidth 0.1 μm	silver in a polymer matrix	752 nm, 200 fs, 76 MHz, NA=1.25	1.59×10^{-6}/3.48 $\times10^{-7}$ Ω m
2009/Cao/Small [39]	NDSS+Ag ions	line/pyramid	MEMS, Metamaterials in visible region	3D: 0.180 μm 2D: 0.120 μm	surfactant-assisted 3D nanostructure	800 nm, 80 fs, 80 MHz, NA=1.4	NA
2010/Xu/Small [78]	silver	flexible nanowiring on nonplanar substrate	MEMS, LoC	0.125 μm	induced electroless plating	790 nm, 120 fs, 82 MHz, NA=1.35	1.6×10^{-7} Ω m
2010/ Ng/Conference-Springer [104]	silver	lines	plastic electronic manufacturing	NP: 100-700 nm wireline: 5 μm	metals on flexible substrates	HeCd laser, 325 nm	7.5×10^{-7} Ω m
2011/Tsutsumi/Appl. Phys. A [69]	silver	lines, helix, pillar, cubic microstructur in a PVP matrix	organic dye laser devices	300-400 nm	effect of molecular weight of PVP on linewidth of silver nanowire is investigated	800 nm, 100 fs, NA=1.3	NA
2011/Terzaki /Opt. Mater. Exp. [2]	MAPTMS +DMAEMA+ ZPO	3D lines	MEMS	NA	silver plating vs. metal bath techniques/coating	800 nm, 20 fs, 75 MHz, NA=0.95, NA=1.4	(1.6±0.1) Ω
2012/Ishikawa /JLMN [50]	silver ion solution	3D/rods	metamaterials, resonant at far infrared 0.9-20.4 THz	0.120 μm	metal ablated from a film/spatial resolution is lower than other methods	800 nm, 80 fs, 82 MHz, NA=1.42	5.30×10^{-8} Ω m
2012/Xu/Nanoscale [74]	gold	lines	thin film based nanoarchitectures	0.560 μm	nanodots precursor instead of metal ions	800 nm, 120 fs, NA=1.35	5.5×10^{-8} Ω m
2012/Furlani/Adv. Optoelectron. [111]	polymer based	chiral	metamaterials	NA	polymer based optical metamaterials	800 nm	NA

(*To be continued on the next page*)

(*Continued*)

Year/Group /Journal	Materials	Structure	Functionality	Resolution	Subject	Beam specification	Resistivity
2012/Vora/JoVE [81]	silver nanostructure inside polymer matrix	dot array	metamaterials, cloaking, perfect lense	0.300 μm	3D nanostructure imbedded in doped PVP	800 nm, 50 fs, 11 MHz, NA=0.8	NA
2012/Vora/Appl. Phys. Lett. [82]	silver	dots	bulk optical devices	300 nm	disconnected silver nanostructures in polymer matrix	795 nm, 50 fs, 11 MHz	NA
2013/Lu/Opt. Mater. Express [72]	gold ion solution	line, u-shaped SRR	metamaterials, resonant at 63 THz-*x*-polarization	0.228 μm	effect of carbon chain length	780 nm, 80 fs, 80 MHz, NA=1.45	16.5×10^{-8} Ω m
2013/Cao/Appl. Phys. Lett. [12]	silver	dots	nanophotonic	0.022 μm	increasing electron donor	800 nm, 140 fs, 80MHz, NA1.4	NA
2015/Wang/Sci. Technol. Adv. Mater [80]	silver NPs	lines	chip/microfluidic chip	wire: 0.19 um silver NPs: tens of nm	controllable assembly of AG-NPs/roughness: 11 nm	800 nm, 120 fs, NA=1.45	NA
2015/Kang/Nanotechnology [11]	silver/gelatin matrix	3D(15)	THz metamaterial devices	Sub 100 nm	3D Ag in a stable dielectric matrix	795 nm, 50 fs, 11 MHz	NA
2015/Gu/Adv. Opt. Matt [11]	silver aqueous solution	2D c-shape array	nanoresonators resonant at 100 & 75 THz	Sub 200 nm	surfactant & photosensitiser assisted 2D nanostructure	532 nm, 250 fs, 50 MHz	1.55 Ω/square

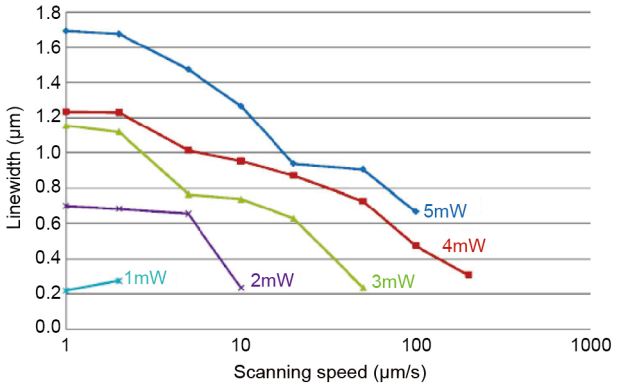

Figure 5 (Color online) Fabrication line width dependence of laser power and scanning speed with a laser of 752 nm wavelength, a pulse width of 200 fs, a repetition rate of 76 MHz, and an objective of 1.25 NA [38].

is higher leading to a lower threshold therefore improved fabrication resolution [53]. On the other hand, the pulse width determines the temporal distribution of the energy. Since the spatial distribution of the focal spot is proportional to the temporal distribution owing to the inclusion of more spectral components [55,64], a shorter pulse can lead to a higher resolution focal spot, which can eventually reduce the fabrication feature size. The laser repletion rate is relevant to the 2PR in terms of the thermal diffusion. Normally a lower repetition rate results in less thermal diffusion effect, which in turn benefits the 2PR fabrication resolution [53].

3 Material for 2PR fabrication

Since materials properties have profound impact on the 2PR fabrication outcomes, it is important to know the material characteristics to optimize the fabrication product. Formulations may vary based on different application requirements. Here we focus on the metallic materials that are useful for plasmonic relevant applications. The conductivity, feature size and surface roughness of the fabricated structures have been used as the basic criteria. In this section, we present a review of different materials that have been used so far in 2PR fabrication. The fabricated structures are discussed considering the resolution, conductivity, surface roughness and also functionality.

Fabrication materials in 2PR can be categorized into two types: one is a metal-ion aqueous solution containing metal salt with dye as the main ingredients; the other one is a metal-ion doped polymeric film. Among all metals, silver is the most popular material to be used in the 2PR fabrication process either as a metal salt to make the aqueous solution or as metal-ions to be doped in polymer films due to different reasons such as its high chemical stability, controllability,

good plasmonic properties and low-cost compared to gold. Commercially available silver salts such as $AgNO_3$, $AgClO_4$ and $AgBF_4$ could be mixed with de-ionized water and eventually with either dye or polymer for preparing aqueous solutions and polymer films, respectively; while for gold structures, $HAuCl_4$ is often used as the metal salt.

The beginning of the study on photoreduction of silver ions dates back to 1976 [65]. A lot of research efforts have been devoted to developing 2PR fabrication technique in the last decade [40,63], which resulted in a rapid progress in this field recently.

Many research groups have used metal-ion doped polymeric films to fabricate metallic structures by 2PR because using polymer can reduce the surface roughness much lower than structures made from the aqueous solution. This is, because metal ions distribute more uniformly in polymer matrix and polymer prevents detrimental metal ion diffusion. According to the state-of-the-art, multidimensional continuous structures have been fabricated in polymeric matrix [38,63,66-68]. These structures show a proper interconnection between NPs which in turn helps to develop the electrical conductivity of the structure; Continuous 2D/3D structures with a smooth, continues surface and resistivity of 3.48×10^{-7} Ω m has been reported by Maruo et al. [38] as the only conductive structure reported among all groups. In their experiment, they used a Ti:Sapphire laser of 752 nm wavelength with a pulse width of 200 fs and a repetition rate of 76 MHz with an 1.25 NA objective, as shown in Figure 6. According to their report only the appropriate amount of the photon density in the focal region and a proper density of silver ions in the polymer matrix could make such continuous lines of 200 nm width. With the same mixture of material but not enough photon and silver density, the final structure would not be smooth and well conductive [68].

In this method, a polymer material, such as polyvinylpyrrolidone (PVP), is used as a polymer matrix and it is dissolved in ethanol. In the second step, silver nitrate is dissolved in deionized water. Polymer solution and silver solution are mixed in the next step and stirred for a while. Eventually, a cover slip is coated with the final solution to make the thin film. The process contains prebake at a high temperature above 100°C after coating, through which silver ions are likely to aggregate and prevents achieving a high spatial resolution [38].

Tsutsumi et al. [69] introduced a polymer based 2PR fabrication method but they performed the fabrication at a laser wavelength of 508 nm, which was different from the usual 780 to 800 nm sensitizer excitation wavelengths, to improve the lateral spatial resolution. In this experiment a femtosecond laser of 800 nm wavelength, a repetition rate of 1 kHz, and a pulse width of 100 fs and an oil immersed objective lens with NA of 1.30 was used and the wavelength was converted to 508 nm wavelength using an optical parametric amplifier (OPA). The light with the wavelength of 508 nm could directly excite the carbonyl group of PVP via the 2PR process and reduce the silver ions. The scanning speed of laser light was 2 μm/s and the laser energy was considered in the range of 6-50 μW. One pair of electrons in PVP-stabilized silver ions and decreased the molecular weight of PVP preventing silver clusters growing larger. As a result, narrow silver clusters of linewidth ranging from 300 to 400 nm were fabricated in the PVP matrix, which was an advancement towards structure resolution improvement.

Although excellent progress in optical properties of metallic microstructures using this method has been achieved, there are still challenges to further advance this technique. For instance, being a multi-step process as shown in Figure 6, it makes this method a time-consuming approach, in addition to the spatial resolution limit of the conductive structures. This might be due to the prebake process.

Metal-ion aqueous solution is introduced to fabricate metallic micro/nanostructures via the 2PR technique by Tanaka et al. [40] Tanaka proposed the fabrication of a self-standing 3D microstructure with high electrical conductivity via the 2PR method using metal-ion aqueous solution. They prepared the aqueous solution of $AgNO_3$ and $HAuCl_4$ for the fabrication of silver and gold structures, respectively. The coverslip was coated with 3-aminopropyltrimethoxysilane to at-

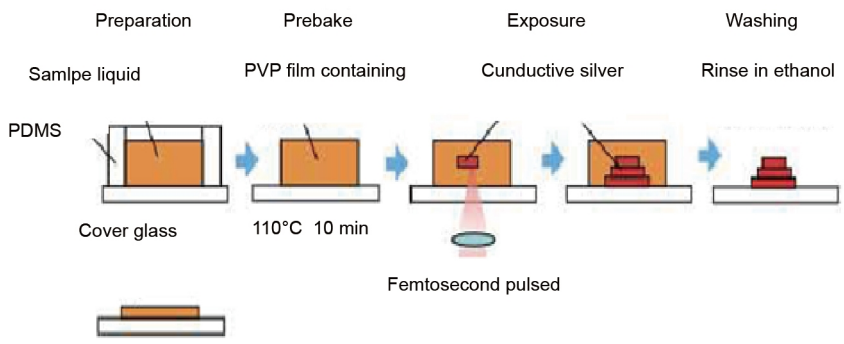

Figure 6 (Color online) Experimental procedure for sample preparation and 3D laser drawing of metallic microstructures using metal-ion doped polymeric films with a laser of 752 nm wavelength, a pulse width of 200 fs, a repetition rate of 76 MHz, and 1.25 NA objective [38].

tach the metal pattern firmly on the substrate surface. According to their report the average resistivity of 5.30×10^{-8} Ω m was achieved. However, the surface roughness was still high and limited the functionality of the structures. Developing the photoreduction material to gain higher electrical conductivity and feature resolution was continued by Ishikawa et al. [70]. They used a two-photon sensitive dye (coumarin 440) in the reduction aqueous solution containing $AgNO_3$ and investigated that the presence of dye could reduce the diameter of the fabricated dots from 3.39 to 0.55 μm, while the required fabrication power changed in the case of the absence and presence of dye from 14.97 to 1.88 mW, respectively. Improvement in resolution for wires fabricated in this work was 400 nm and 3D structure of free-standing rod was successfully fabricated. In 2008 by modifying photoreduction material Cao et al. [39] could fabricate silver strips with the linewidth of 120 nm and 3D structure with the size of 180 nm, which is the best resolution reported to date based on the TPR technique. They succeeded in achieving such a result by adding nitrogen-atom containing alkyl carboxylate n-decanoyl sarcosine sodium (NDSS) as the surfactant to the reduction solution to prevent the growth of unwanted silver particles. This way, they provided a simple method to precisely control the position of NPs, in addition to the efficient creation and accumulation of the NPs.

As mentioned previously, to enable functionalities in nanophotonics, microelectronics, and MEMS technology, metallic microstructures need to be well controlled on the size of the aggregated NPs and the surface smoothness.

Cao et al. [71] proposed the method to fabricate the structures with respect to the different carbon chain lengths (C_n: n= 4, 5, 7, 9) of fatty salt in the photoreduction as shown in Figures 7(a)-(h). A mode-locked Ti:Sapphire laser (Tsunami, Spectra Laser), which provided a pulse width of 80 fs, a wavelength of 800 nm as well as a repetition rate of 80 MHz. The laser beam was introduced into an inversed microscope (IX-71, Olympus) and tightly focused into the sample solution placed on a cover slip by an oil-immersed objective lens (×60) with a high numerical aperture (NA = 1.4, Olympus). The fatty salts used in the sample solutions include sodium valerate with four carbons in its chain (C4), sodium hexanoate (C5), sodium caprylate (C7) and sodium decanoate (C9). According to the results increasing the chain length from C4 to C9 results in increasing the resolution from about 600 to 450 nm. Also it can improve the surface smoothness, which has a key role in making the structure efficient for low-loss photonics applications. The reason for this is a larger hydrophobic force existing in the longer carbon chain chemical, which prevents the growth of NPs efficiently.

Ishikawa [50] reported the first fabrication of 2D functional metallic nanostructure for plasmonics metamaterials in 2012. The silver rod-pair array was fabricated using the same TPR technique and the same mixture of the aqueous solution as mentioned above by this group. Magnetic resonances with negative permeability at the far-infrared frequency were demonstrated by these silver rod pair array. This was the starting point on the functionality track of metallic micro/nanostructures towards micro/nanodevice fabrication using the 2PR technique, which has been improved further since then. In 2013, Lu et al. [72] fabricated gold nanostructures using a new stabilizer, amino-terminated ionic liquid with $AuCl^-_4$ ions. NPs with sizes less than 5 nm were achieved, which eventually lead to the high smoothness of the fabricated structure. The fabricated u-shape planar metamaterials of 228 nm line width showed a spectral response in the terahertz region, which achieved another milestone towards the fabrication of microphotonics/electronic devices. However, the structure was not responding to the polarization of incident light, which in turn limits the potential applications, although the calculated electrical resistivity of 16.5×10^{-8} Ω m was achieved, which is in the same order of magnitude as that of bulk gold.

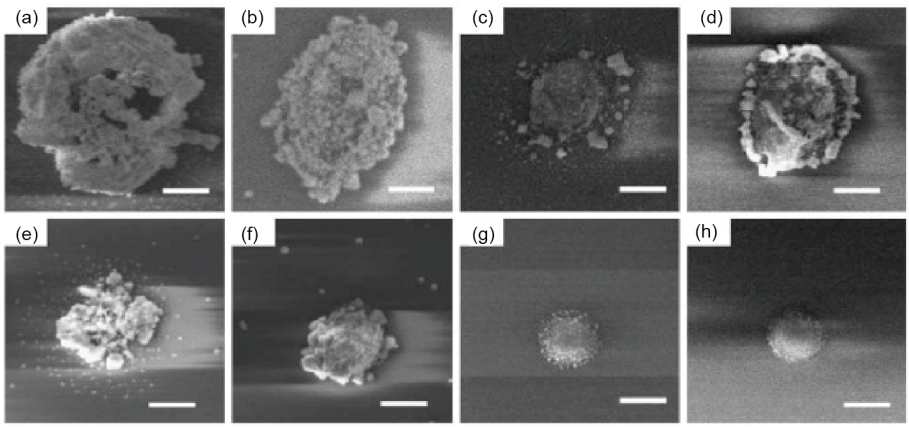

Figure 7 (a)-(d) SEM images of the silver dots fabricated in sample solutions with different faty salts: (a) for C_4, (b) for C_5, (c) for C_7, and (d) for C_9, which are under the laser power of 4.6 mW and the laser wavelength of 800 nm; (e)-(h) SEM images of the silver dots fabricated in sample solutions with different faty salts: (e) for C_4, (f) for C_5, (g) for C_7, and (h) for C_9, under the laser power of 1.3 mW and the laser wavelength of 800 nm; scale bars: (a)-(h) 500 nm [71].

Although, promising and exciting progresses have been reported so far from various research groups in this field, there are still key challenges to achieve an excellent functional metallic nanostructure. From the functionality point of view, there is always a discrepancy in conductivity between bulk silver and fabricated silver nanostructures because of oxidization, sulfurization and also the surface roughness which degrade the functionality of the structure. The same challenges exist for fabricating gold nanostructures.

In fact, the fabricated structures are the pile of the NPs and they are not like the bulk metal with high crystalline structure. Therefore, the conductivity is quite low [72]. The inclusion of organic or other residual chemicals such as surfactants [39,47,72] and photoinitiator [73] also reduces the conductivity, although their presence in the solution decreases the size of the produced NPs. On the other hand, the pile of the particles increases the surface roughness, which introduces losses for electrons [40,74]. These problems can be potentially solved by reducing the NPs size to nanometer range less than 10 nm [12,71,72,75] and allow them to densely packed together by tunning the carbon chain length [71,75] thermal annealing or even with tighter focusing [47,76], which can also remove the organic chemicals if there is any remaining.

Recently, functional silver plasmonic resonators that are responsive to light polarization have been demonstrated [47]. The fabricated silver c-shaped array has a low root-mean-square surface roughness of 22 nm, small sheet resistance of 1.55 Ω/square and high feature resolution of less than 200 nm, leading to measured optical resonances in the near to mid-infrared region. The aqueous solution was prepared with mixing three components: a photosensitizer, a growth inhibitor and a source of silver. A water soluble dye (2-hydroxy-4'-(2-hydroxyethoxy)-2-methylpropiophenone (HHMP)) was used as the photosensitizer and a surfactant NDSS was used as the growth inhibitor, which improved the fabrication resolution in the TPR process. The conductivity of the structure can potentially be tuned by changing the concentration of the growth inhibitor to prevent the formation of the insulating layer on the metal NPs [12]. Therefore, the achievement of the functional plasmonic structures via the 2PR process has manifested the importance of controlling NPs size on the improvement of the feature resolution, conductivity and surface smoothness. It is obvious, the smaller the NP size is, the higher the achievable resolution, surface smoothness and conductivity is, if no insulating layer is involved on the surface of the NPs. Hence, to achieve a functional metallic nanostructure via the 2PR process a great attention should be dedicated to controlling the NP size. Using metal-ion doped polymer films for 2PR makes it quite challenging the sizes of NPs to be reached less than 50 nm [12,72]. While fabrication in aqueous solution under optimized conditions enables the formation of NPs in a scale less than 50 nm, establishing an excellent platform for high resolution metallic structure with a great smoothness and a high conductivity. NP size can be adjusted by controlling the level of light confinement in the focal region. The stronger light confines the faster reduction process it will lead to, which results in the decrease of the NP size.

4 State-of-the-art of 2PR structures

It is important to characterize the fabricated structures regarding their physical properties such as electrical conductivity, surface roughness, fabrication resolution and optical properties in order to evaluate their functionalities. Hence, a brief review has been provided in this section due to the significance of characterization as the final stage of the experiment, which can guide researchers to optimize the fabrication products.

4.1 Conductivity

In the experiment, there are two main methods for characterizing the electrical conductivity of the fabricated structures and their composites. Either a digital voltmeter or a four-point probe can be used in this case. To measure the electrical conductivity through a digital voltmeter, usually two metallic electrode pads are fabricated of silver, gold or cupper on a glass substrate and then metallic lines can be fabricated via the 2PR process between them to connect the electrodes as shown in Figure 8. Eventually, the resistivity can be calculated using the measured resistance from the gradient of the current versus the applied voltage and the geometrical parameters of lines such as length, width, and height [40,72].

The latter method with a four-point probe is usually used to characterize a large area or a thin film [47]. Since the distance between the two end-probes in a four-point probe tool is 4 mm, the structure should be at least in a 4 mm area according to the Figure 9.

Measurement of the sheet resistivity with a four-point probe is through the following equation:

$$\rho_{\text{square}}\left(\frac{\Omega}{\text{square}}\right)=\frac{\pi}{\ln(2)}\frac{V}{I}. \tag{3}$$

For the bulk resistivity measurement, we need to consider the bulk thickness as well, so the equation has a very small variation as below:

$$\rho=\frac{\pi}{\ln(2)}t\left(\frac{V}{I}\right)=4.523t\left(\frac{V}{I}\right). \tag{4}$$

According to the state of the art, the acceptable and the best range of reported resistivity obtained via these methods is on the order of 10^{-8}-10^{-6} Ω m (bulk silver and gold resistivity order), which supports the functionality of the structures for

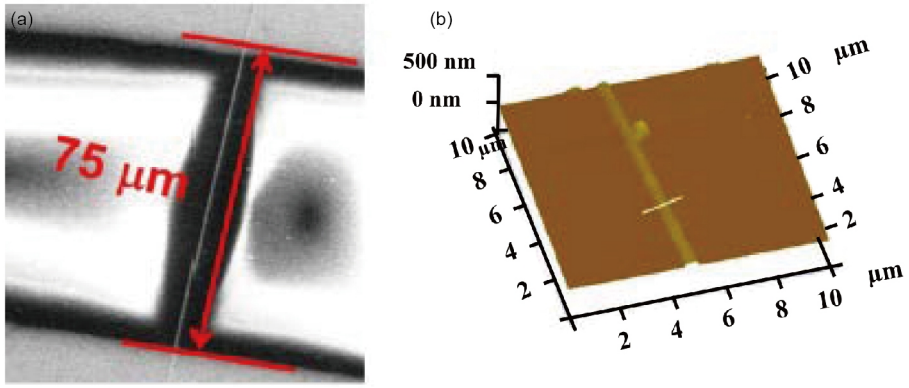

Figure 8 (Color online) (a) SEM image of a gold metallic nano line between two Au electrodes. (b) AFM image of the gold nano line [72].

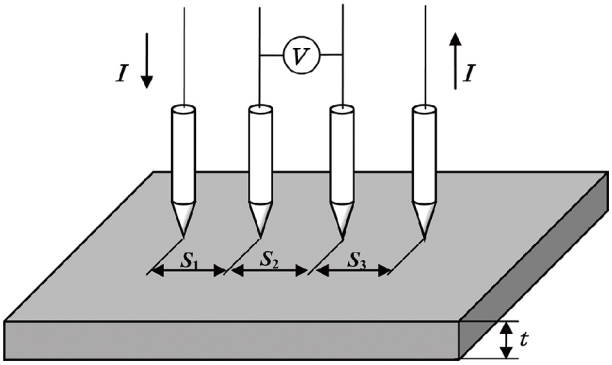

Figure 9 Schematic of a four-point probe for sheet resistivity measurement [77].

the different level of applications.

4.2 Resolution

The resolution and morphology of the fabricated structures could be characterized by various microscopes, including a scanning electron microscopy (SEM) or a transmission electron microscopy (TEM). According to Table 1, the best-achieved resolution of the fabricated silver dots via 2PR is 22 nm [12], which could be potentially used to produce nanophotonics/electronic devices for sensing and SERS applications. The best-reported resolution for line fabrication is around 120 nm [39,50,78] for applications such as integration of microcircuits in MEMS, LoC, microfluidic devices and plasmonics and metamaterials resonantor at far-field in the THz region [47,79]. As is discussed earlier in this section, controlling the growth of NPs during the 2PR process is of great value to improve the resolution of linewidth in the structure. So in addition to the material properties, laser parameters also need to be optimized to target different types of applications [72,80,81].

4.3 Surface roughness

The surface roughness of the fabricated structure is characterized by atomic force microscopy (AFM). Surface roughness level is determined by the average roughness over a certain area. As an example, the topography and cross-sections of silver lines fabricated via 2PR are shown in Figures 10(d)-(i) [39].

AFM characterization provides the measurement of the surface roughness of the structure. Different level of smoothness is necessary for the different range of applications. For instance, plasmonic structures and metamaterials need a highly smooth surface of below 100 nm roughness to be responsive effectively to incident light with a low loss [47].

5 Applications

As has been discussed extensively in this section, 2PR can be a versatile technique to fabricate metallic micro/nanostructures, which have a great potential to be applied in many applications such as plasmonics, metamaterials, nanowires, microfluidics chips, LoC devices and also as SERS substrates. Different research groups have reported the fabrication of plasmonic structures—such as grating-like, disconnected and connected nanostructures [11,27,82,83], metamaterials [72,84-96], which can bend, scatter, transmit or otherwise shape EM radiation in ways that no natural material can. Here we provide a summary of the applications of multidimensional micro/nanostructures fabricated through the 2PR method.

5.1 SERS substrates

Since the SERS was used for single molecule detection due to its strong enhancement, different methods have been introduced to fabricate SERS substrates for a larger field enhancement [97,98]. Among all the approaches the 2PR process is known as the most repeatable and reliable method to prepare SERS substrates in a cost-effective manner. With a femtosecond laser at the optimized fabrication conditions, regularly arranged grating-like nanostructures were directly fabricated and silver NPs could form on the nanostructure simultaneously with high enhancement factor (EF) of 10^9 via a one-step

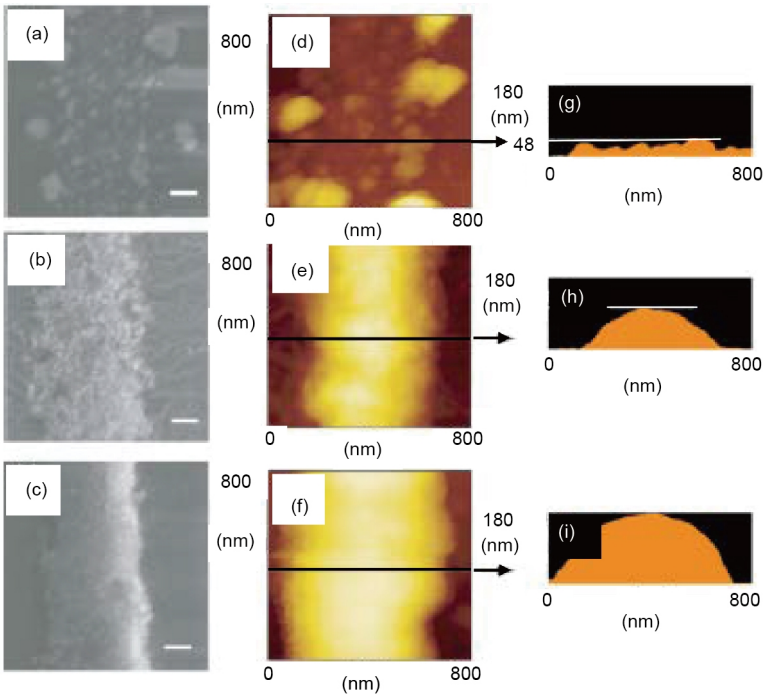

Figure 10 (Color online) The left column contains SEM images obtained from samples with [NDSS]= (a) 0.013 M, (b) 0.033 M, and (c) 0.099 M, respectively; (d)-(f) show corresponding topography and (g)-(i) show cross-sectional images taken by AFM. Scale bars are 100 nm in (a), (b), and (c) [39].

fabrication technique [79,99-101]. This new method for fabrication of multifunctional integrated microchips and SERS substrate has a great potential application for LoC technology [60]. Xu et al. [102] successfully fabricated localized flexible integration of SERS monitors. The patterned silver substrate at the bottom of a microchannel was fabricated through 2PR with a high enhancement factor of ~10^8. The 2PR process allows the design of flexible structures that could form unique SERS substrates into various patterns and could be placed at any desired point of the microchannels. This group also fabricated on-chip silver microflower arrays within the microfluidic channel as a catalytic microreactor to allow *in situ* SERS monitoring via 2PR [103]. The fabricated structure shows a high catalytic activity and SERS enhancement of ~10^8.

5.2 Flexible electronics

Direct fabrication of 3D metallic micro/nanostructure is the most significant advantage of the 2PR technique comparing to other photolithography methods.

It has been investigated that complex geometries could be fabricated by 2PR into photoreduction solution on the planar substrate. Moreover, 2PR affords to fabricate the design on either nonplanar substrate or on the flexible substrate; which broadens the application spectra and makes this fabrication technique extremely powerful. Xu et al. [78] succeeded to demonstrate flexible metal nanowire on nonplanar substrate as shown in Figure 11(a). Also, they provided the fabrication of microheater inside the microchannels for microfluidic applications as shown in Figure 11(b). The patterned silver nanowires maintained a low resistivity of about $1.6\times10^{-7}\,\Omega$ m, that makes it a great candidate for circuitry and electronic interconnection applications that required a high conductivity, for instance as a heating circuit.

Ng et al. [104] reported on the fabrication of a helical silver track written onto a cylindrical polyimide substrate as shown in Figure 12(a). This process has introduced a low-cost manufacturing method for 2.5D structures such as spiral inductors used in components as capacitors or inter-digital electrodes in Figure 12(b). Although this process needs several steps to be completed, the potential of 2PR has been confirmed for fabricating micro/nanostructures on a flexible and nonplanar substrate.

5.3 Microfluidic devices

Microfluidic chips or LoC systems are widely used in synthesis, analysis, detection, sensing and therapy in various field such as biology, chemistry, physics, material science, pharmaceuticals because of its integrated multifunctional system [79,105].

When SERS is combined with LoC, a sensitive system can be created for optofluidic detection. Integration of solid-state SERS substrate with microfluidic devices (Figures 13(a)-(d)) could be realized through two different methods. One way is the chemical route and the other is the laser micro/nanofabrication technique. With the help of DLW, 3D complex structure could be fabricated in a broad range of materials. Xu et al. [103] presented nanoflower array fabricated via 2PR inside the microfluidic channel for a catalytic reaction.

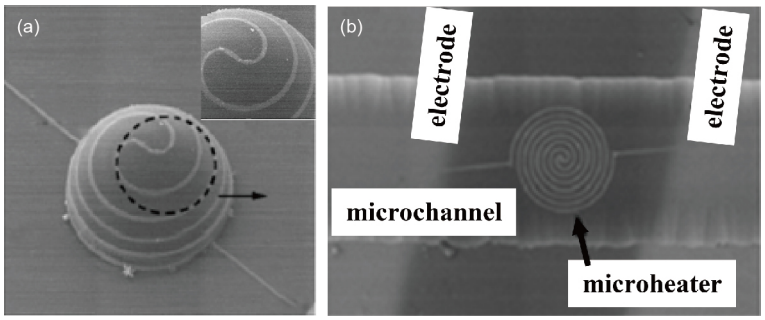

Figure 11 (a) SEM image of the silver microwinding on a hemisphere, (b) SEM image of silver microheater inside a microchannel (80 μm in width and 20 μm in depth) [78].

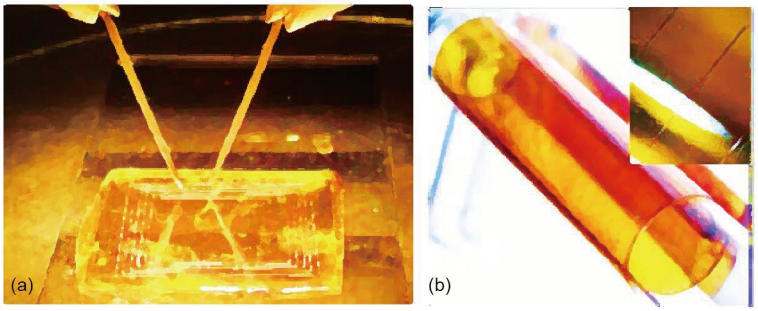

Figure 12 (Color online) (a) An electroless Cu plated micro-coil fabricated by DLW. (b) Long silver helix track fabricated by a laser on glass pipette coated with a polyimide film. Inset shows the magnified image of the track with a linewidth of 15 μm [104].

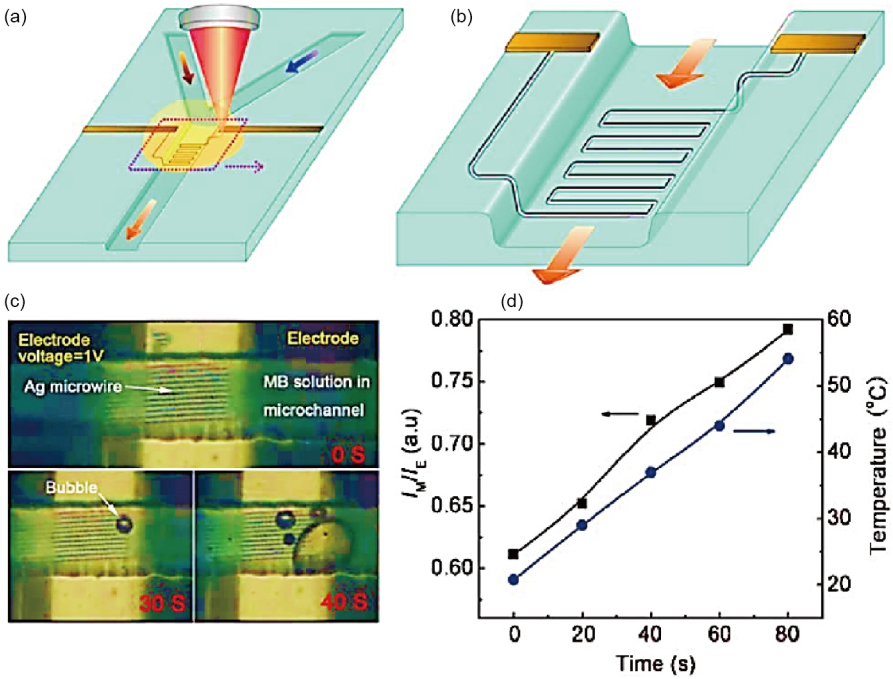

Figure 13 (Color online) (a), (b) Schematic illustration of the fabrication of a silver microheater inside a microfluidic channel. (c) Heating test of a microheater fabricated inside a microchannel. Optical micrographs of the heating process. (d) The intensity ratio of monomer to excimer of PS-Na used to quantitatively calculate the local temperature and dependence of temperature on heating time [105].

According to the literature, one of the major challenges in the fabrication of microfluidic devices and integration with solid-state SERS substrate is the high cost and sophisticated fabrication method, which can be solved with the 2PR technique. In addition, 2PR technique could aid miniaturization of SERS-enabled LoC systems to achieve a portable detection system. Moreover, the powerful 2PR technique could also offer the design and integration of more functional units dra-

matically increasing the functionality and complexity. Considering the advances in 2PR fabrication in the near future, it is promising to expand application ranges for microfluidic chips.

5.4 Plasmonic and metamaterials

Using the 2PR method, the first functional planar metamaterials structure was made by Lu et al. [72] in 2013. The fabricated u-shape gold resonance rings with a laser of 780 nm wavelength—demonstrates a quite smooth surface as shown in Figure 14(a)—a low resistivity of 16.5×10^{-8} Ω m was achieved. Optical characterization of the structure with an FTIR confirms a electric resonance around 63 THz for the *x*-polarized wave. However, no *y*-polarization resonance was observed according to the Figure 14(b).

Tabrizi et al. [47] successfully fabricated functional plasmonic resonators via 2PR at a laser wavelength of 532 nm. High resolution silver c-shape of 200 nm linewidth demonstrated highly smooth surface of 22 nm RMS (Figure 15(a)) with a low sheet reistance of 1.55 Ω/square; which are necassery for plasmonic functionality. The optical properties such as transmission and absorption of light considering different polarization of light by the structure are characterized by Fourier Transform Infrared (FTIR) spectroscopy. Silver c-shape structure was responsive to external light polarizations in two directions at 75 THz and 100 THz as shown in Figure 15(b); and moreover was tunable in a large dynamic range by changing the laser fabrication parameters.

6 Conclusion and outlook

Apart from all the above-mentioned methods to improve the feature resolution in 2PR fabrication, performing super resolution technique can develop resolution impressively. Gan et al. [76] reported 3D optical beam lithography fabrication with 9 nm feature size and 52 nm two-line resolution in a developed non-metallic two-photon absorption resin with high mechanical strength. According to the super resolution method, two-beam of optical beam lithography has the advantage of fabricating 3D arbitrary geometry with nanometer feature size and resolution comparable to EBL by the photo inhibition strategy. If fabricating metallic structure with this method would be possible, DLW based on 2PR can be the winner in the competition with EBL technique due to its ability in cost-effectiveness and simple fabrication of 3D arbitrary geometry with nanometer feature size. Utilizing this method can bring a revolution in metallic nanofabrication technology.

Except high-resolution feature, mass production is another concern for nanofabrication of 3D structures. Parallel writing could considerably increase the throughput of the DLW method and make 2PR one of the most promising future nanofabrication technologies [12,41,106]. In principle, it is possible to perform a spatial light modulator (SLM) or a multiple mirror array (MMA) to fabricate different structures at different points in the focal plane simultaneously [38]. According to the literature, multifocal fabrication of split ring array is possible using SLM enables laser fabrication of microstructures. Polymer SR array with a single exposure process was fabricated as shown in Figure 16 [107]. Combining the direct laser printing (DLP) technique with the 2PR method provides a viable routine to realize high throughput high resolution fabrication of functional metallic nanodevices.

As mentioned in the beginning of this article, achieving advanced functionality, for example the 3D chirality, it is essential to achieve 3D functional metallic structures, which could be potentially realized via the 2PR method. Although some 3D metallic microstructures have been fabricated by the 2PR, no real functionality has been demonstrated [39,40,108]. In this method, any arbitrary 3D structure should be fabricated in such conditions that all nanoparticles pack densely enough to resist surface tension during washing process. However, in most of the cases the roughness of the structures prevents any meaningful attempt to achieve real functionalities. One

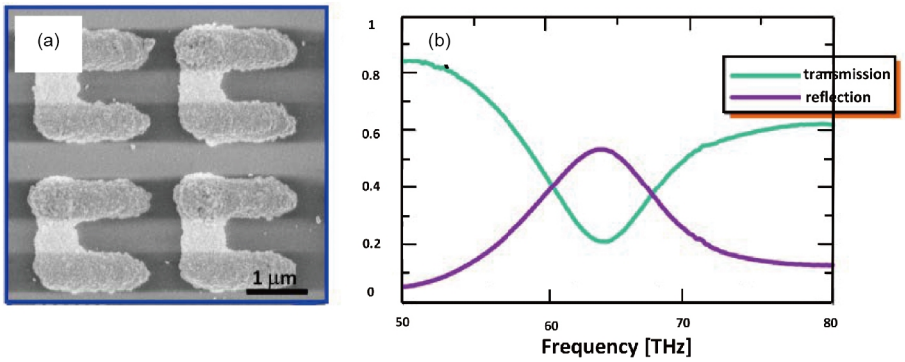

Figure 14 (Color online) (a) SEM image of the u-shape gold resonance rings on glass substrate, which was fabricated under the laser power of 1.57 mW and the scanning speed of 2 μm/s using the sample solution with Length=1.9 μm, Height=150 nm, Width=640 nm, Periodicity=3 μm. (b) Measured transmission and reflection spectra for the metamaterials with *x*-polarized illumination [72].

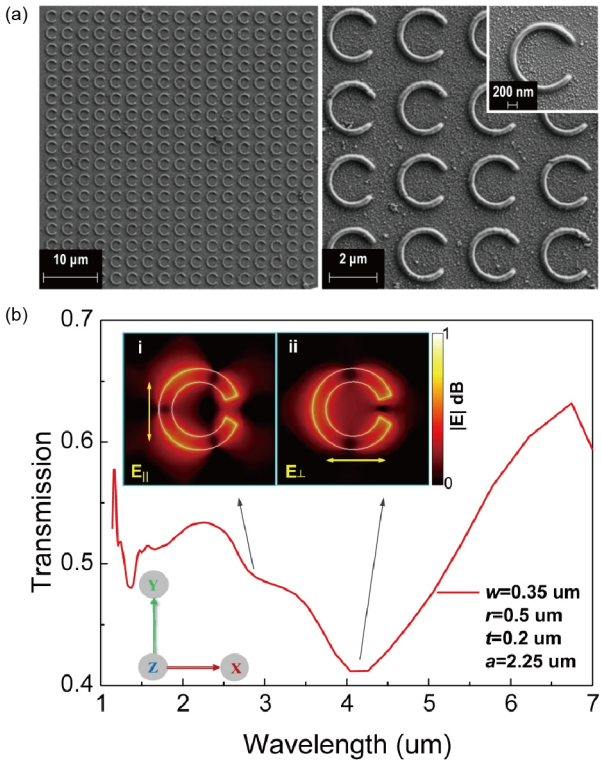

Figure 15 (Color online) (a) SEM images of fabricated c-shape arrays showing a 200 nm linewidth and excellent smoothness. (b) Transmission spectrum of a c-shape array with parameters listed in the figure showing two distinct dips in transmission that are attributed to the two Mie-type resonances when the polarization is (i) parallel to the gap and (ii) perpendicular to the gap [47].

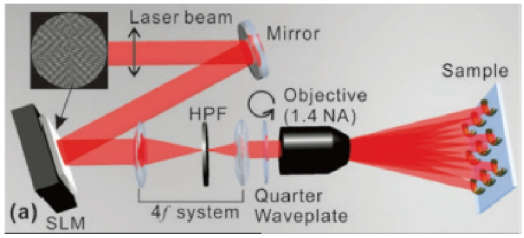

Figure 16 (Color online) Experimental setup for the DLP nanofabrication system for polymer SR structures. The arrow indicates the polarization direction of the laser beam. Top left inset: the displayed phase modulation [107].

possible reason is due to the fabrication based on the scanning along the *z*-direction. Because during scanning of each point either over exposing or extra thermal distribution affects the previous spot and degrades the uniformity of the size, shape and spacing of nanoparticles. So the final structure forms no functionality. Consequently, if we can prevent this situation by single shot fabrication of the entire structure using an SLM assisted DLP method [106,107], it might be useful to fabricate highly uniform 3D structures with a proper continuity that demonstrate good functionality. In principle, it is possible to arbitrarily shape the beam in the focal region by using an SLM.

In summary, using a simple and low-cost 2PR method, functional multidimensional metallic micro/nanostructures with sufficient quality could be formed for a variety type of applications such as nanowires, SERS, microfluidic chips, LoC, plasmonics and metamaterials. These functional structures are readily tunable in a large dynamic range by simply changing the laser fabrication parameters. However, further advancements rely on both superresolution, parallel writing as well as more conductive and sensitive material development. We believe combining this versatile direct laser reduction technique with the superresolution and parallel writing methods will lead to a new laser-based fabrication platform enabling multidimensional functional artificial material fabrication in future.

This work was supported by the Australian Research Council through the Discovery Early Career Researcher Award Scheme (Grant No. DE120100291), and the Discovery Project Scheme (Grant No. DP150102972).

1 N. C. Lindquist, P. Nagpal, K. M. McPeak, D. J. Norris, and S. H. Oh, Rep. Prog. Phys. **75**, 036501 (2012).
2 K. Terzaki, N. Vasilantonakis, A. Gaidukeviciute, C. Reinhardt, C. Fotakis, M. Vamvakaki, and M. Farsari, Opt. Mater. Express **1**, 586 (2011).
3 X. M. Duan, H. B. Sun, K. Kaneko, and S. Kawata, Thin Solid Films **453-454**, 518 (2004).
4 H. Hidai, and H. Tokura, Appl. Surface Sci. **174**, 118 (2001).
5 D. Kim, S. Jeong, B. K. Park, and J. Moon, Appl. Phys. Lett. **89**, 264101 (2006).
6 A. Gupta, and R. Jagannathan, Appl. Phys. Lett. **51**, 2254 (1987).
7 T. Cacouris, G. Scelsi, P. Shaw, R. Scarmozzino, R. M. Osgood, and R. R. Krchnavek, Appl. Phys. Lett. **52**, 1865 (1988).
8 A. Radke, T. Gissibl, T. Klotzbücher, P. V. Braun, and H. Giessen, Adv. Mater. **23**, 3018 (2011).
9 S. Shukla, X. Vidal, E. P. Furlani, M. T. Swihart, K. T. Kim, Y. K. Yoon, A. Urbas, and P. N. Prasad, ACS Nano **5**, 1947 (2011).
10 Y. Son, T. W. Lim, D. Y. Yang, P. Prabhakaran, K. S. Lee, J. Bosson, O. Stephan, and P. L. Baldeck, IJNM **6**, 219 (2010).
11 S. Y. Kang, K. Vora, and E. Mazur, Nanotechnology **26**, 121001 (2015).
12 Y. Cao, and M. Gu, Appl. Phys. Lett. **103**, 213104 (2013).
13 R. P. Seisyan, Tech. Phys. **56**, 1061 (2011).
14 L. J. Guo, Adv. Mater. **19**, 495 (2007).
15 C. Vieu, F. Carcenac, A. Pépin, Y. Chen, M. Mejias, A. Lebib, L. Manin-Ferlazzo, L. Couraud, and H. Launois, Appl. Surface Sci. **164**, 111 (2000).
16 L. A. Giannuzzi, and F. A. Stevie, Micron **30**, 197 (1999).
17 X. Luo, and T. Ishihara, Appl. Phys. Lett. **84**, 4780 (2004).
18 N. Fang, H. Lee, C. Sun, and X. Zhang, Science **308**, 534 (2005).
19 P. Gao, N. Yao, C. Wang, Z. Zhao, Y. Luo, Y. Wang, G. Gao, K. Liu, C. Zhao, and X. Luo, Appl. Phys. Lett. **106**, 093110 (2015).
20 T. C. Chong, M. H. Hong, and L. P. Shi, Laser Photon. Rev. **4**, 123 (2010).
21 D. B. Chrisey, A. Pique, J. Fitz-Gerald, R. C. Y. Auyeung, R. A. McGill, H. D. Wu, and M. Duignan, Appl. Surface Sci. **154-155**, 593 (2000).
22 M. M. Hossain, G. Chen, B. Jia, X. H. Wang, and M. Gu, Opt. Express **18**, 9048 (2010).
23 M. M. Hossain, and M. Gu, Laser Photon. Rev. **8**, 233 (2014).

24 B. Jia, J. Li, and M. Gu, Aust. J. Chem. **60**, 484 (2007).
25 B. Kaehr, N. Ertaş, R. Nielson, R. Allen, R. T. Hill, M. Plenert, and J. B. Shear, Anal. Chem. **78**, 3198 (2006).
26 J. Li, B. Jia, G. Zhou, and M. Gu, Opt. Express **14**, 10740 (2006).
27 Y. L. Zhang, Q. D. Chen, H. Xia, and H. B. Sun, Nano Today **5**, 435 (2010).
28 E. B. Kley, Microelectronic Eng. **34**, 261 (1997).
29 F. Korte, J. Serbin, J. Koch, A. Egbert, C. Fallnich, A. Ostendorf, and B. N. Chichkov, Appl. Phys. A **77**, 229 (2003).
30 C. N. LaFratta, D. Lim, K. O'Malley, T. Baldacchini, and J. T. Fourkas, Chem. Mater. **18**, 2038 (2006).
31 L. Li, M. Hong, M. Schmidt, M. Zhong, A. Malshe, B. Huis in't Veld, and V. Kovalenko, CIRP Ann.-Manuf. Tech. **60**, 735 (2011).
32 H. E. Williams, Z. Luo, and S. M. Kuebler, Opt. Express **20**, 25030 (2012).
33 Q. Z. Zhao, J. R. Qiu, X. W. Jiang, E. W. Dai, C. H. Zhou, and C. S. Zhu, Opt. Express **13**, 2089 (2005).
34 H. B. Sun, and S. Kawata, J. Lightw. Technol. **21**, 624 (2003).
35 W. Zhang, and Y. L. Yao, J. Manuf. Sci. Eng. **124**, 369 (2002).
36 J. K. Gansel, M. Thiel, M. S. Rill, M. Decker, K. Bade, V. Saile, G. von Freymann, S. Linden, and M. Wegener, Science **325**, 1513 (2009).
37 N. Liu, H. Guo, L. Fu, S. Kaiser, H. Schweizer, and H. Giessen, Nat. Mater. **7**, 31 (2008).
38 S. Maruo, and J. T. Fourkas, Laser Photon. Rev. **2**, 100 (2008).
39 Y. Y. Cao, N. Takeyasu, T. Tanaka, X. M. Duan, and S. Kawata, Small **5**, 1144 (2009).
40 T. Tanaka, A. Ishikawa, and S. Kawata, Appl. Phys. Lett. **88**, 081107 (2006).
41 J. Li, M. M. Hossain, B. Jia, D. Buso, and M. Gu, Opt. Express **18**, 4491 (2010).
42 Y. G. Bi, J. Feng, Y. F. Li, Y. L. Zhang, Y. S. Liu, L. Chen, Y. F. Liu, L. Guo, S. Wei, and H. B. Sun, ACS Photon. **1**, 690 (2014).
43 Y. L. Zhang, L. Guo, H. Xia, Q. D. Chen, J. Feng, and H. B. Sun, Adv. Opt. Mater. **2**, 10 (2014).
44 D. Lau, and S. Furman, Appl. Surface Sci. **255**, 2159 (2008).
45 L. Huang, Y. Liu, L. C. Ji, Y. Q. Xie, T. Wang, and W. Z. Shi, Carbon **49**, 2431 (2011).
46 B. Li, X. Zhang, X. Li, L. Wang, R. Han, B. Liu, W. Zheng, X. Li, and Y. Liu, Chem. Commun. **46**, 3499 (2010).
47 S. Tabrizi, Y. Cao, B. P. Cumming, B. Jia, and M. Gu, Adv. Opt. Mater. **4**, 529 (2016).
48 N. V. Tkachenko, *Optical Spectroscopy: Methods and Instrumentations* (Elsevier, Amsterdam, 2006).
49 A. V. Kachynski, A. Pliss, A. N. Kuzmin, T. Y. Ohulchanskyy, A. Baev, J. Qu, and P. N. Prasad, Nat. Photon **8**, 455 (2014).
50 A. Ishikawa, JLMN **7**, 11 (2012).
51 S. A. Maier, *Plasmonics: Fundamentals and Applications* (Springer Science & Business Media, Berlin, Heidelberg, Dordrecht, and New York, 2007).
52 G. S. He, G. C. Xu, P. N. Prasad, B. A. Reinhardt, J. C. Bhatt, and A. G. Dillard, Opt. Lett. **20**, 435 (1995).
53 K. Miura, J. R. Qiu, T. Mitsuyu, and K. Hirao, Proc. SPIE, **3618**, 141 (1999).
54 J. Qiu, Chem. Record **4**, 50 (2004).
55 Y. Li, S. Chemerisov, and J. Lewellen, Phys. Rev. ST Accel. Beams **12**, 020702 (2009).
56 D. W. Lewis, *Resource Conservation by Use of Iron and Steel Slags*, in *Extending Aggregate Resources* (American Society for Testing and Materials, 1982), pp. 31-42.
57 Q. Liu, X. Duan, and C. Peng, *Novel optical technologies for nanofabrication* (Springer, New York, 2014).
58 M. Sakamoto, M. Fujistuka, and T. Majima, J. Photochem. Photobio. C-Photochem. Rev. **10**, 33 (2009).
59 M. Bom, and E. Wolf, *Principles of Optics* (Pergamon, New York, 1980), pp. 747-754.
60 Z. Zhou, J. Xu, Y. Liao, Y. Cheng, Z. Xu, K. Sugioka, and K. Midorikawa, Opt. Commun. **282**, 1370 (2009).
61 A. S. Quick, H. Rothfuss, A. Welle, B. Richter, J. Fischer, M. Wegener, and C. Barner-Kowollik, Adv. Funct. Mater. **24**, 3571 (2014).
62 E. Kymakis, K. Savva, M. M. Stylianakis, C. Fotakis, and E. Stratakis, Adv. Funct. Mater. **23**, 2742 (2013).
63 K. Kaneko, H. B. Sun, X. M. Duan, and S. Kawata, Appl. Phys. Lett. **83**, 1426 (2003).
64 W. J. Brown, S. G. Anderson, C. P. J. Barty, S. M. Betts, R. Booth, J. K. Crane, R. R. Cross, D. N. Fittinghoff, D. J. Gibson, F. V. Hartemann, E. P. Hartouni, J. Kuba, G. P. Le Sage, D. R. Slaughter, A. M. Tremaine, A. J. Wootton, P. T. Springer, and J. B. Rosenzweig, Phys. Rev. ST Accel. Beams **7**, 060702 (2004).
65 H. Hada, Y. Yonezawa, Y. Yoshida Akio, and A. Kurakake, J. Phys. Chem. **80**, 2728 (1976).
66 B. Fisette, and M. Meunier, Proc. SPIE, **5578**, 677 (2004).
67 F. Stellacci, C. A. Bauer, T. Meyer-Friedrichsen, W. Wenseleers, V. Alain, S. M. Kuebler, S. J. K. Pond, Y. Zhang, S. R. Marder, and J. W. Perry, Adv. Mater. **14**, 194 (2002).
68 T. Baldacchini, A. C. Pons, J. Pons, C. N. Lafratta, J. T. Fourkas, Y. Sun, and M. J. Naughton, Opt. Express **13**, 1275 (2005).
69 N. Tsutsumi, K. Nagata, and W. Sakai, Appl. Phys. A **103**, 421 (2011).
70 A. Ishikawa, T. Tanaka, and S. Kawata, Appl. Phys. Lett. **89**, 113102 (2006).
71 Y. Y. Cao, X. Z. Dong, N. Takeyasu, T. Tanaka, Z. S. Zhao, X. M. Duan, and S. Kawata, Appl. Phys. A **96**, 453 (2009).
72 W. E. Lu, Y. L. Zhang, M. L. Zheng, Y. P. Jia, J. Liu, X. Z. Dong, Z. S. Zhao, C. B. Li, Y. Xia, T. C. Ye, and X. M. Duan, Opt. Mater. Express **3**, 1660 (2013).
73 T. Itakura, K. Torigoe, and K. Esumi, Langmuir **11**, 4129 (1995).
74 B. B. Xu, R. Zhang, H. Wang, X. Q. Liu, L. Wang, Z. C. Ma, Q. D. Chen, X. Z. Xiao, B. Han, and H. B. Sun, Nanoscale **4**, 6955 (2012).
75 W. E. Lu, M. L. Zheng, W. Q. Chen, Z. S. Zhao, and X. M. Duan, Phys. Chem. Chem. Phys. **14**, 11930 (2012).
76 Z. Gan, Y. Cao, R. A. Evans, and M. Gu, Nat. Commun. **4**, 2061 (2013).
77 F. M. Smits, Bell Syst. Technical J. **37**, 711 (1958).
78 B. B. Xu, H. Xia, L. G. Niu, Y. L. Zhang, K. Sun, Q. D. Chen, Y. Xu, Z. Q. Lv, Z. H. Li, H. Misawa, and H. B. Sun, Small **6**, 1762 (2010).
79 B. B. Xu, Y. L. Zhang, H. Xia, W. F. Dong, H. Ding, and H. B. Sun, Lab Chip **13**, 1677 (2013).
80 H. Wang, S. Liu, Y. L. Zhang, J. N. Wang, L. Wang, H. Xia, Q. D. Chen, H. Ding, and H. B. Sun, Sci. Tech. Adv. Mater. **16**, 024805 (2015).
81 K. Vora, S. Y. Kang, and E. Mazur, JoVE **69**, UNSP e4399 (2012).
82 K. Vora, S. Y. Kang, S. Shukla, and E. Mazur, Appl. Phys. Lett. **100**, 063120 (2012).
83 R. Ameloot, M. B. J. Roeffaers, G. De Cremer, F. Vermoortele, J. Hofkens, B. F. Sels, and D. E. De Vos, Adv. Mater. **23**, 1788 (2011).
84 D. R. Smith, W. J. Padilla, D. C. Vier, S. C. Nemat-Nasser, and S. Schultz, Phys. Rev. Lett. **84**, 4184 (2000).
85 N. Engheta, and R. W. Ziolkowski, *Metamaterials: Physics and Engineering Explorations* (John Wiley & Sons, Hoboken, 2006).
86 S. Zouhdi, S. Ari, and P. Alexey, *Metamaterials and Plasmonics: Fundamentals, Modelling, Applications* (Springer Science & Business Media, Berlin, Heidelberg, Dordrecht, and New York, 2008).
87 E. Plum, X. X. Liu, V. A. Fedotov, Y. Chen, D. P. Tsai, and N. I. Zheludev, Phys. Rev. Lett. **102**, 113902 (2009).
88 F. Capolino, *Theory and Phenomena of Metamaterials* (CRC Press, New York, 2009).
89 A. Vallecchi, S. Campione, and F. Capolino, J. Nanophoton **4**, 041577 (2010).
90 R. Marques, F. Mesa, J. Martel, and F. Medina, IEEE Trans. Antennas Propagat. **51**, 2572 (2003).

91 R. Liu, T. J. Cui, D. Huang, B. Zhao, and D. R. Smith, Phys. Rev. E **76**, 026606 (2007).
92 C. Caloz, and T. Itoh, *Electromagnetic Metamaterials: Transmission Line Theory and Microwave Applications* (John Wiley & Sons, Hoboken, 2005).
93 A. K. Iyer, P. C. Kremer, and G. V. Eleftheriades, Opt. Express **11**, 696 (2003).
94 V. M. Shalaev, Nat. Photon. **1**, 41 (2007).
95 T. M. Grzegorczyk, and J. A. Kong, J. Electromag. Waves Appl. **20**, 2053 (2006).
96 W. Xu, L. W. Li, H. Y. Yao, T. S. Yeo, and Q. Wu, J. Electromag. Waves Appl. **20**, 13 (2006).
97 S. A. Maier, Opt. Express **14**, 1957 (2006).
98 M. Moskovits, J. Raman Spectrosc. **36**, 485 (2005).
99 C. H. Lin, L. Jiang, Y. H. Chai, H. Xiao, S. J. Chen, and H. L. Tsai, Opt. Express **17**, 21581 (2009).
100 I. Izquierdo-Lorenzo, S. Jradi, and P. M. Adam, RSC Adv. **4**, 4128 (2014).
101 S. J. Lee, B. D. Piorek, C. D. Meinhart, and M. Moskovits, Nano Lett. **10**, 1329 (2010).
102 B. B. Xu, Z. C. Ma, L. Wang, R. Zhang, L. G. Niu, Z. Yang, Y. L. Zhang, W. H. Zheng, B. Zhao, Y. Xu, Q. D. Chen, H. Xia, and H. B. Sun, Lab Chip **11**, 3347 (2011).
103 B. B. Xu, R. Zhang, X. Q. Liu, H. Wang, Y. L. Zhang, H. B. Jiang, L. Wang, Z. C. Ma, J. F. Ku, F. S. Xiao, and H. B. Sun, Chem. Commun. **48**, 1680 (2012).
104 J. G. Ng, D. E. G. Watson, J. Sigwarth, A. McCarthy, H. Suyal, D. P. Hand, and M. P. Y. Desmulliez, *An Additive Method for Photopatterning of Metals on Flexible Substrates*, in *Proceedings of the 36th International MATADOR Conference* (Springer, London, 2010), pp. 389-392.
105 J. A. Huang, Y. L. Zhang, H. Ding, and H. B. Sun, Adv. Opt. Mater. **3**, 618 (2015).
106 H. Lin, B. Jia, and M. Gu, Opt. Lett. **36**, 406 (2011).
107 H. Lin, and M. Gu, Appl. Phys. Lett. **102**, 084103 (2013).
108 F. Formanek, N. Takeyasu, T. Tanaka, K. Chiyoda, A. Ishikawa, and S. Kawata, Opt. Express **14**, 800 (2006).
109 E. T. Castellana, S. Kataoka, F. Albertorio, and P. S. Cremer, Anal. Chem. **78**, 107 (2006).
110 S. Maruo, and T. Saeki, Opt. Express **16**, 1174 (2008).
111 E. P. Furlani, H. S. Jee, H. S. Oh, A. Baev, and P. N. Prasad, Adv. OptoElectron. **2012**, 1 (2012).